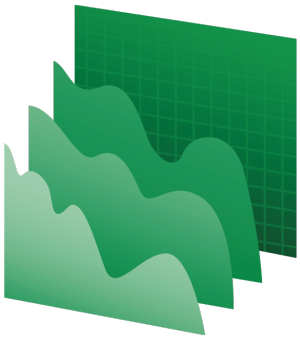

Match-up database Analyses Report

SMOS-L2-DPGS-v662

TSG-GOSUD-Sailing-ship

Global Ocean

prepared by the Pi-MEP Consortium

May 15, 2018

Contents

Acronym

Aquarius	NASA/CONAE Salinity mission
ASCAT	Advanced Scatterometer
ATBD	Algorithm Theoretical Baseline Document
BLT	Barrier Layer Thickness
CMORPH	CPC MORPHing technique
CTD	Instrument used to measure the conductivity, temperature, and pressure of seawater
DM	Delayed Mode
EO	Earth Observation
ESA	European Space Agency
FTP	File Transfer Protocol
GOSUD	Global Ocean Surface Underway Data
GTMBA	The Global Tropical Moored Buoy Array
Ifremer	Institut français de recherche pour l'exploitation de la mer
IPEV	Institut polaire français Paul-Émile Victor
IQR	Interquartile range
ISAS	In Situ Analysis System
L2	Level 2
LEGOS	Laboratoire d'Etudes en Géophysique et Océanographie Spatiales
LOCEAN	Laboratoire d'Océanographie et du Climat : Expérimentations et Approches Numériques
LOPS	Laboratoire d'Océanographie Physique et Spatiale
MDB	Match-up database
MEOP	Marine Mammals Exploring the Oceans Pole to Pole
MLD	Mixed Layer Depth
NRT	Near Real Time
Pi-MEP	Pilot Mission Exploitation Platform
PIRATA	Prediction and Researched Moored Array in the Atlantic
QC	Quality control
R_{sat}	Spatial resolution of the satellite SSS product
RAMA	Research Moored Array for African-Asian-Australian Monsoon Analysis and Prediction
RR	Rain rate
SAMOS	Shipboard Automated Meteorological and Oceanographic System
SMAP	Soil Moisture Active Passive (NASA mission)
SMOS	Soil Moisture and Ocean Salinity (ESA mission)
SSS	Sea Surface Salinity
SSS_{insitu}	In situ SSS data considered for the match-up
SSS_{SAT}	Satellite SSS product considered for the match-up
ΔSSS	Difference between satellite and in situ SSS at colocalized point ($\Delta SSS = SSS_{SAT} - SSS_{insitu}$)
SST	Sea Surface Temperature
STD	Standard deviation
Survostral	SURVeillance de l'Océan AuSTRAL (Monitoring the Southern Ocean)
TAO	Tropical Atmosphere Ocean
TSG	Thermosalinograph

1 Overview

In this report, we present systematic analyses of the Match-up DataBase (MDB) files generated by the Pi-MEP platform within the following Pi-MEP region and for the below pair of Satellite/In situ SSS data:

- Pi-MEP region: Global Ocean
- SSS satellite product (SSS_{SAT}): SMOS-L2-DPGS-v662
- In situ dataset (SSS_{Insitu}):TSG-GOSUD-Sailing-ship

In the following, $\Delta SSS = SSS_{SAT} - SSS_{Insitu}$ denotes the difference between the satellite and in situ SSS at the colocalized points that form the MDB.

This report presents successively:

The MDB file DataSets (Section 2)

- A short description of the satellite SSS product considered in the match-up (2.1)
- A short description of the In situ SSS dataset considered in the match-up (2.2)
- A short description of the auxiliary geophysical datasets co-localized with SSS pairs (2.3)
- An overview of how the Match-ups were evaluated (2.4)
- An overview of the MDB characteristics for the particular in situ/satellite pairs (2.5)

The major results of the MDB file Analyses (Section 3)

- Spatial Maps of the Time-mean and temporal STD of in situ and satellite SSS and of the ΔSSS (3.1)
- Time series of the monthly averaged mean and STD of in situ and satellite SSS and of the ΔSSS (3.2)
- Zonally-averaged Time-mean and temporal STD of in situ and satellite SSS and of the ΔSSS (3.3)
- Scatterplots of satellite vs in situ SSS by latitudinal bands (3.4)
- Time series of the monthly averaged mean and STD of the ΔSSS sorted by latitudinal bands (3.5)
- ΔSSS sorted as function of geophysical conditions (3.6)

All analyses are conducted over the Pi-MEP Region specified above and over the full satellite SSS product period.

2 The MDB file datasets

2.1 Satellite SSS product

2.1.1 SMOS-L2-DPGS-v662

Quality and major features of the SMOS Level 2 Sea Surface Salinity data products generated by version 662 of the Level 2OS Operational Processor (L2OS) can be found in the SMOS-Level-2-Ocean-Salinity-v662-release-note. Version 662 of the Level 2 Sea Surface Salinity data product is available for the SMOS mission lifetime with the following file class and version:

File class	File version	From	To
REPR	V662	1 June 2010	09 May 2017
OPER	V662	10 May 2017	present

The data set acquired during the SMOS mission commissioning phase (from January 2010 to 31 May 2010) has been acquired during periods when the MIRAS instrument underwent several tests and was operated in different modes, causing drifts not fully compensated by the on-ground calibration processing. For that reason, this data set has not been reprocessed with the latest version of the L2OS processor. The SMOS data users are invited to use this new data set, which supersedes the previous one generated by the algorithm baseline version 622 and to read this note carefully to ensure optimum exploitation of the version 662 data set. Further information on the quality of the data set can be found in the reprocessing reports for data quality control available here and for data verification available here.

Main improvements in the L2OS version 662 data set

The major improvements introduced in the currently operational version 662 of the SMOS Level 2 sea surface salinity processor are:

1. Modified User Data Product (UDP) containing salinities retrieved using only the roughness model previously known as model 1, or SSS1, which has now been selected as the reference model for estimating the sea roughness contribution to brightness temperature. Salinities retrieved using roughness models 2 and 3 are still available in the Data Analysis Product (DAP).

2. A new salinity product corrected for land-sea contamination (LSC) (SSS_corr). Contamination of L1 brightness temperatures when the instrument images a scene that includes a land-sea transition in the FOV (up to 1000 km from the coast) has been shown to introduce significant errors (up to 2 pss) in salinity fields. For a full description, see Annex 5 in the Algorithm Theoretical Baseline Document (ATBD), available here. Bias correction LUTs (so called mixed-scene LUTs) have been generated from a long time series of L1 data for both ascending and descending orbits and are applied to L1 brightness temperatures before retrieval of SSS_corr. The method used to derive the se land-sea contamination correction LUTs is described in section 2.2.8 of the Table Generation Requirement Document (TGRD), available here. If land-sea contamination correction has been applied to any of the measurements used during SSS_corr retrieval, a flag (Fg_ctrl_mixed_scene) is set. Salinities retrieved without land-sea correction (SSS_uncorr) are also available in the UDP.

3. New (experimental) salinity anomaly product (SSS_anom) computed from SSS_corr and WOA 2009 climatology (SSS_anom = SSS_corr minus WOA 2009). Daily interpolated climatology is computed from the monthly WOA 2009 LUT before extracting SSS_anom.

ESL s plan to develop a SMOS-based climatology to be used in future versions of the L2OS processor, with the objective of providing a de-biased SSS anomaly field.

4. New scene-based filtering algorithm to mitigate contamination from RFI and other sources (e.g., sun), based on a set of metrics comparing differences between brightness temperatures of successive snapshots including a complete polarization cycle (so-called scenes). A scene is defined in section 2.2.8.2 of the TGRD, and the scene-based filtering algorithm is described in section 2.2.8.4 of the TGRD, available here.

5. New sun glint model and sun brightness temperatures LUTs used as part of the forward model, and to set sun glint flags more accurately. Operational (OPER) products use a constant sun brightness temperature, whereas the reprocessed products (REPR) use a daily estimated L-band sun brightness temperature LUT for orbits prior to 22 November 2016.

6. Roughness model 1 LUT has been updated by ESL, improving the estimation of forward model roughness brightness temperatures at wind speeds > 12 m/s.

7. TEC retrieved from SMOS 3rd Stokes polarimetric measurements used for both ascending and descending orbits (for both sea surface salinity retrievals and OTT computation), to provide an improved Faraday rotation estimation.

8. Acard parameter computed with land-sea corrected L1 brightness temperatures and the complete forward model including flat sea, roughness model 1, galactic and sun glint components.

9. Modified UDP format : see Tables below. Land sea contamination corrected salinities and associated fields/flags have suffix "_corr"; uncorrected salinities have suffix "_uncorr"; whilst anomalies have suffix "_anom". For further details of the new UDP format see tables 47, 48 and 49 in section 3.2.6 of the Input/Output Data Definition Document (IODD) available here.

10. Updated configuration of switches and filters used in the data processing. For further information see the section 2.4.7 of the TGRD, available here. The L2OS version 662 data set has been generated using the same L1c data set as the previous L2OS version 622 data set: i.e., L1c data version 620. For further details on the L1c data sets see the L1c data version 620 read-me-first note available here: here

L2OS version 662 performance and caveats

The reprocessed data set has been analysed by ESLs and ARGANS. The reference document is mentioned above. The main conclusions are:

- Land-sea contamination corrected salinities (SSS_corr) almost cancel the global mean bias in near -to-coast regions (> 40 km and < 800 km) compared to SSS_uncorr. Also, there are more valid SSS_corr retrievals near to the coast than in SSS_uncorr (the LSC correction allows retrieval of previously contaminated pixels). However, in regions with high RFI (e.g. China seas, NW Indian Ocean, DEW line - see RFI probability maps from CESBIO: http://www.cesbio.upstlse.fr/SMOS_blog/smos_rfi/) or natural geophysical variability (e.g. river plumes), land-sea contamination correction is either unavailable (due to insufficient data to compute the land-sea correction LUT) or unreliable (due to a mismatch between WOA climatology and rapid salinity variability). In these regions, SSS_corr is prone to inaccuracies (see also plots in Section 5 below).

- Globally, the novel scene-based filtering and updated roughness model 1 determine an increase in the number of retrievals in both ascending and descending orbits. The new sun glint model also allows an increase in the number and quality of retrievals at the edge of the swath during periods of high sun glint (e.g., western edge of southern hemisphere descending orbits, in November-January) and high sun L-band intensity (2012-2015).
- The new experimental salinity anomaly product is still experimental, as the WOA 2009 climatology is not always directly related to SMOS surface salinities, especially in regions of high variability (e.g., ITCZ). ESLs plan to derive a SMOS based climatology for future anomaly products, to provide a field intrinsically devoid of systematic errors. The El-Niño event of 2015-2016 is visible in Pacific region ascending and descending orbit Hovmoller plots (see Section 2.4.1 in the L2OS v662 reprocessing verification report).
- Across-track biases and ascending-descending differences still remain. Retrievals near to the edge of the swath (x_swath $> \pm$ 350 km) have higher uncertainties due to the smaller number of measurements, and contamination from various sources, especially sun aliases and associated ripples (tails). Ascending orbits have less bias than descending (see across-track Hovmoller plots in the L2OS v662 reprocessing verification report), while descending passes have stronger biases during January March and October-December periods.
- ESLs have reported that there is evidence of residual inaccuracies in salinity retrievals due to TEC and galactic glint modelling issues. Therefore, users should be aware that salinities retrieved during periods of high TEC activity (corresponding to high solar activity, especially for descending orbits) and high galactic glint (see sections 5.2 and 5.5 in the L2OS Reprocessing Report) are less accurate.
- Strong latitudinal bias in SSS_corr can be seen in the Northern Hemisphere during March-May in both ascending and descending orbits (see global Hovmoller plots in figures 18 and 20 in the L2OS v662 re processing verification report), but these are not visible in SSS_uncorr. Similar latitudinal biases can also be seen in SSS_anom for Pacific and Atlantic regions (see Hovmoller plots in figures 35-39 in the L2OS v662 reprocessing report). Therefore, land-sea contamination corrected salinities (and anomalies) above 30N during these periods exhibit worse performance than elsewhere or in different periods of the year.

Filtering retrievals

We strongly recommend users to filter L2OS sea surface salinity retrievals using one of the following set of criteria:

1. For best quality data: Dg_quality_SSS < 150
2. For more data but with lower quality : Fg_ctrl_poor_geophysical $= 0$ and Fg_ctrl_poor_retrieval $= 0$
3. Other combinations of UDP flags and filters including at least Fg_ctrl_chi2 $= 0$ or Fg_ctrl_chi2_P $= 0$
4. Other filters used by the L2OS Expert Support Laboratories for generating Level 3 salinity maps as described in the L2OS v662 reprocessing verification report sections 2.1 and 2.2, available here.

Flags used before MDB files generation
We only select data in the MDB files such as the following conditions or flags are met:

- Dg_quality_SSS < 150
- Dg_af_fov > 130
- control_flag_set: CTRL_ECMWF
- control_flag_clear: CTRL_NUM_MEAS_MIN, CTRL_NUM_MEAS_LOW, CTRL_MANY_OUTLIERS, CTRL_SUNGLINT, CTRL_MOONGLINT, CTRL_REACH_MAXITER, CTRL_MARQ, CTRL_CHI2_P, CTRL_SUSPECT_RFI
- science_flag_set: SC_LOW_WIND, SC_LAND_SEA_COAST1
- science_flag_clear: SC_ICE, SC_SUSPECT_ICE

Satellite SSS product characteristics

Table 1: Satellite SSS product characteristics

SMOS-L2-DPGS-v662	
Spatial resolution	∼40 km
Temporal repeat	3 days
Temporal coverage	From 2010-06-01 to now
Spatial coverage	Global [-180 180 -90 90]
Data Provider	ESA
Version	662
ATBD	SMOS_L2OS-ATBD
Data access	level-2-ocean-salinity

2.2 In situ SSS dataset

The TSG-GOSUD-Sailing-ship dataset correspond to Observations of Sea surface salinity obtained from voluntary sailing ships using medium or small size sensors. They complement the networks installed on research vessels or commercial ships. This delayed mode dataset (Reynaud et al. (2015)) is updated annually as a contribution to GOSUD (`http://www.gosud.org`) and freely available here. Adjusted values when available and only collected TSG data that exhibit quality flags=1 and 2 were used.

2.3 Auxiliary geophysical datasets

Additional EO datasets are used to characterize the geophysical conditions at the in situ/satellite SSS pair measurement locations and time, and 10 days prior the measurements to get an estimate of the geophysical condition and history. As discussed in Boutin et al. (2016), the presence of vertical gradients in, and horizontal variability of, sea surface salinity indeed complicates comparison of satellite and in situ measurements. The additional EO data are used here to get a first estimates of conditions for which L-band satellite SSS measured in the first centimeters of the upper ocean within a 50-150 km diameter footprint might differ from pointwise in situ

measurements performed in general between 10 and 5 m depth below the surface. The spatio-temporal variability of SSS within a satellite footprint (50–150 km) is a major issue for satellite SSS validation in the vicinity of river plumes, frontal zones, and significant precipitation. Rainfall can in some cases produce vertical salinity gradients exceeding 1 pss m^{-1}; consequently, it is recommended that satellite and in situ SSS measurements less than 3–6 h after rain events should be considered with care when used in satellite calibration/validation analyses. To identify such situation, the Pi-MEP test platform is first using CMORPH products to characterize the local value and history of rain rate and ASCAT gridded data are used to characterize the local surface wind speed and history.

2.3.1 CMORPH

Precipitation are estimated using the CMORPH 3-hourly products at 1/4° resolution (Joyce et al. (2004)). CMORPH (CPC MORPHing technique) produces global precipitation analyses at very high spatial and temporal resolution. This technique uses precipitation estimates that have been derived from low orbiter satellite microwave observations exclusively, and whose features are transported via spatial propagation information that is obtained entirely from geostationary satellite IR data. At present NOAA incorporate precipitation estimates derived from the passive microwaves aboard the DMSP 13, 14 and 15 (SSM/I), the NOAA-15, 16, 17 and 18 (AMSU-B), and AMSR-E and TMI aboard NASA's Aqua, TRMM and GPM spacecraft, respectively. These estimates are generated by algorithms of Ferraro (1997) for SSM/I, Ferraro et al. (2000) for AMSU-B and Kummerow et al. (2001) for TMI. Note that this technique is not a precipitation estimation algorithm but a means by which estimates from existing microwave rainfall algorithms can be combined. Therefore, this method is extremely flexible such that any precipitation estimates from any microwave satellite source can be incorporated.

With regard to spatial resolution, although the precipitation estimates are available on a grid with a spacing of 8 km (at the equator), the resolution of the individual satellite-derived estimates is coarser than that - more on the order of 12 x 15 km or so. The finer "resolution" is obtained via interpolation.

In effect, IR data are used as a means to transport the microwave-derived precipitation features during periods when microwave data are not available at a location. Propagation vector matrices are produced by computing spatial lag correlations on successive images of geostationary satellite IR which are then used to propagate the microwave derived precipitation estimates. This process governs the movement of the precipitation features only. At a given location, the shape and intensity of the precipitation features in the intervening half hour periods between microwave scans are determined by performing a time-weighting interpolation between microwave-derived features that have been propagated forward in time from the previous microwave observation and those that have been propagated backward in time from the following microwave scan. NOAA refer to this latter step as "morphing" of the features.

For the present Pi-MEP products, we only considered the 3-hourly products at 1/4 degree resolution. The entire CMORPH record (December 2002-present) for 3-hourly, 1/4 degree lat/lon resolution can be found at: `ftp://ftp.cpc.ncep.noaa.gov/precip/CMORPH_V1.0/RAW/`. CMORPH estimates cover a global belt (-180°W to 180°E) extending from 60°S to 60°N latitude and are available for the complete period of the Pi-MEP core datasets (Jan 2010-now).

2.3.2 ASCAT

Advanced SCATterometer (ASCAT) daily data produced and made available at Ifremer/CERSAT on a 0.25°x0.25° resolution grid (Bentamy and Fillon (2012)) since November 2008 are used to

characterize the mean daily wind at the match-up pair location as well as the wind history during the 10-days period preceding the in situ measurement date. These wind fields are calculated based on a geostatistical method with external drift. Remotely sensed data from ASCAT are considered as observations while those from numerical model analysis (ECMWF) are associated with the external drift. The spatial and temporal structure functions for wind speed, zonal and meridional wind components are estimated from ASCAT retrievals. Furthermore, the new procedure includes a temporal interpolation of the retrievals based on the complex empirical orthogonal function (CEOF) approach, in order to enhance the sampling length of the scatterometer observations. The resulting daily wind fields involves the main known surface wind patterns as well as some variation modes associated with temporal and spatial moving features. The accuracy of the gridded winds was investigated through comparisons with moored buoy data in Bentamy et al. (2012) and resulted in rms differences for wind speed and direction are about 1.50 m.s^{-1} and 20°.

2.3.3 ISAS

The In Situ Analysis System (ISAS), as described in Gaillard et al. (2016) is a data based reanalysis of temperature and salinity fields over the global ocean. It was initially designed to synthesize the temperature and salinity profiles collected by the ARGO program. It has been later extended to accommodate all type of vertical profile as well as time series. ISAS gridded fields are entirely based on in-situ measurements. The methodology and configuration have been conceived to preserve as much as possible the data information content and resolution. ISAS is developed and run in a research laboratory (LOPS) in close collaboration with Coriolis, one of ARGO Global Data Assembly Center and unique data provider for the Mercator operational oceanography system. At the moment the period covered starts in 2002 and only the upper 2000m are considered. The gridded fields were produced over the global ocean 70°N–70°S on a 1/2° grid by the ISAS project with datasets downloaded from the Coriolis data center (for more details on ISAS see Gaillard et al. (2009)). In the PiMEP, the product in used is the INSITU_GLO_TS_OA_NRT_OBSERVATIONS_013_002_a v6.2 NRT derived at the Coriolis data center and provided by Copernicus (www.marine.copernicus.eu/documents/PUM/CMEMS-INS-PUM-013-002-ab.pdf). The major contribution to the data set is from Argo array of profiling floats, reaching an approximate resolution of one profile every 10-days and every 3-degrees over the Satellite SSS period (`http://www.umr-lops.fr/SNO-Argo/Products/ISAS-T-S-fields/`); in this version SSS from thermosalinographs from ship of opportunity are not used, so that we can consider SMOS SSS validation using ship of opportunity measurements independent of ISAS. The ISAS optimal interpolation involves a structure function modeled as the sum of two Gaussian functions, each associated with specific time and space scales, resulting in a smoothing over typically 3 degrees. The smallest scale which can be retrieved with ISAS analysis is not smaller than 300–500 km (Kolodziejczyk et al. (2015)). For validation purpose, the ISAS monthly SSS fields at depth level 5 m are collocated and compared with the satellite SSS products and included in the PiMEP MDB files. In addition, the « percentage of variance » fields (PCTVAR) contained in the ISAS analyses provide information on the local variability of in situ SSS measurements within 1/2°x1/2° boxes.

2.3.4 World Ocean Atlas Climatology

The World Ocean Atlas 2013 version 2 (WOA13 V2) is a set of objectively analyzed (1° grid) climatological fields of in situ temperature, salinity and other variables provided at standard depth levels for annual, seasonal, and monthly compositing periods for the World Ocean. It also includes associated statistical fields of observed oceanographic profile data interpolated to

standard depth levels on 5°, 1°, and 0.25° grids. We use these fields in complement to ISAS to characterize the climatological fields (monthly mean and std) at the match-up pairs location and date.

2.4 Overview of the Match-ups generation method

The match-up production is basically a three steps process:

1. preparation of the input in situ and satellite data, and,
2. co-localization of satellite products with in situ SSS measurements.
3. co-localization of the in situ/satellite pair with auxiliary information.

In the following, we successively detail the approaches taken for these different steps.

2.4.1 In Situ/Satellite data filtering

The first step consist in filtering TSG-GOSUD-Sailing-shipin situ dataset using the quality flags as described in 2.2 so that only valid salinity data remains in the produced match-ups.

For high-spatial resolution in situ SSS measurements such as the Thermo-SalinoGraph (TSG) SSS data from research vessels, Voluntary Observing Ships (VOS) or sailing ships, as well as SSS data from surface drifters, an additional spatial-filtering step is performed on the in situ data that will be in fine compared to the satellite SSS products. If R_{sat} is the spatial resolution of the satellite SSS product (L2 to L3-L4), we keep the in situ data at the original spatial resolution but we also estimate for all spatio-temporal samples a running median filtered SSS applied to all neighbouring in situ SSS data acquired within a distance of $R_{sat}/2$ from a given in situ acquisition. Both the original and the filtered data are finally stored in the MDB files.

Only for satellite L2 SSS data, a third step consist in filtering spurious data using the flags and associated recommendation as provided by the official data centers and described in 2.1.

2.4.2 In Situ/Satellite Co-localization

In this step, each SSS satellite acquisition is co-localized with the filtered in situ measurements. The method used for co-localization differ if the satellite SSS is a swath product (so-called Level 2-types) or a time-space composite product (so-called Level 3/level 4-types).

- For L2 SSS swath data :

  If R_{sat} is the spatial resolution of the satellite swath SSS product, for each in situ data sample collected in the Pi-MEP database, the platform searches for all satellite SSS data found at grid nodes located within a radius of $R_{sat}/2$ from the in situ data location and acquired with a time-lag from the in situ measurement date that is less or equal than $\pm$ 6 hours. If several satellite SSS samples are found to meet these criteria, the final satellite SSS match-up point is selected to be the closest in time from the in situ data measurement date. The final spatial and temporal lags between the in situ and satellite data are stored in the MDB files.

- For L3 and L4 composite SSS products :

  If R_{sat} is the spatial resolution of the composite satellite SSS product and D the period over which the composite product was built (e.g., periods of 1, 7, 8, 9, 10, 18 days, 1 month, etc..) with central time to, for each in situ data sample collected in the Pi-MEP database

during period D, the platform searches for all satellite SSS data of the composite product found at grid nodes located within a radius of $R_{sat}/2$ from the in situ data location. If several satellite SSS product samples are found to meet these criteria, the final satellite SSS match-up point is chosen to be the composite SSS with central time to which is the closest in time from the in situ data measurement date. The final spatial and temporal lags between the in situ and satellite data are stored in the MDB files.

2.4.3 MDB pair Co-localization with auxiliary data and complementary information

MDB data consist of satellite and in-situ SSS pair datasets but also of auxiliary geophysical parameters such as local and history of wind speed and rain rates, as well as various information (climatology, distance to coast, mixed layer depth, barrier layer thickness, etc) that can be derived from in situ data and which are included in the final match-up files. The collocation of auxiliary parameters and additional information is done for each filtered in-situ SSS measurement contained in the match-up files as follows :

If t_{insitu} is the time/date at which the in situ measurement is performed, we collect:

- The ASCAT wind speed product of the same day than t_{insitu} found at the ASCAT 1/4° grid node with closest distance from the in situ data location and the time series of the ASCAT wind speed at the same node for the 10 days prior the in situ measurement day.
- If the in situ data is located within the 60°N-60°S band, we select the CMORPH 3-hourly product the closest in time from tin situ and found at the CMORPH 1/4° grid node with closest distance from the in situ data location. We then store the time series of the CMORPH rain rate at the same node for the 10 days prior the in situ measurement time.

For the given month/year of the in situ data, we select the ISAS and WOA fields for the same month (and same year for ISAS fields) and take the SSS analysis (monthly mean, std) found at the grid node the closest from the in situ measurement.

The distance from the in situ SSS data location to the nearest coast is evaluated and provided in kms. We use a distance-to-coast map derived by CLS with a spatial resolution of 1/16° that we re-gridded at 1/4° resolution taking the minimum value of all 1/16° observations found in the 1/4° grid cell.

When vertical profiles of S and T are made available from the in situ measurements used to build the match-up (Argo or sea mammals), the following variables are included into each satellite/in situ match-up file:

1. The vertical distribution of pressure at which the profile were measured,
2. The vertical S(z) and T(z) profiles,
3. The vertical potential density anomaly profile $\sigma_0(z)$,
4. The Mixed Layer Depth (MLD). The MLD is defined here as the depth where the potential density has increased from the reference depth (10 meter) by a threshold equivalent to 0.2°C decrease in temperature at constant salinity: $\sigma_0 = \sigma_{010m} + \Delta\sigma_0$ with $\Delta\sigma_0 = \sigma_0(\theta_{10m} - 0.2, S_{10m}) - \sigma_0(\theta_{10m}, S_{10m})$ where θ_{10m} and S_{10m} are the temperature and salinity at the reference depth (i.e. 10 m) (de Boyer Montégut et al. (2004), de Boyer Montégut et al. (2007)).
5. The Top of the Thermocline Depth (TTD) is defined as the depth at which temperature decreases from its 10 m value by 0.2°C.

6. The Barrier Layer if present, is defined as the intermediate layer between the top of the thermocline and the bottom of the density mixed-layer and its thickness (BLT) is defined as the difference between the MLD and the TTD.

7. The vertical profile of the buoyancy frequency $N^2(z)$

The resulting match-ups files are serialized as NetCDF-4 files whose structure depends on the origin of the in-situ data they contain.

2.4.4 Content of the Match-Up NetCDF files

netcdf pimep-mdb_smos-l2-v662_tsg-gosud-sailing-ship_20100116_v01 {
dimensions:
TIME_SAT = UNLIMITED ; // (1 currently)
TIME_TSG = 2190 ;
N_DAYS_WIND = 10 ;
N_3H_RAIN = 80 ;
STRING25 = 25 ;
STRING8 = 8 ;

variables:
float DATE_TSG(TIME_TSG) ;
DATE_TSG:long_name = ”Date of TSG” ;
DATE_TSG:units = ”days since 1990-01-01 00:00:00” ;
DATE_TSG:standard_name = ”time” ;
DATE_TSG:_FillValue = -999.f ;
float LATITUDE_TSG(TIME_TSG) ;
LATITUDE_TSG:long_name = ”Latitude of TSG” ;
LATITUDE_TSG:units = ”degrees_north” ;
LATITUDE_DRIFTER:valid_min = -90. ;
LATITUDE_TSG:valid_max = 90. ;
LATITUDE_TSG:standard_name = ”latitude” ;
LATITUDE_TSG:_FillValue = -999.f ;
float LONGITUDE_TSG(TIME_TSG) ;
LONGITUDE_TSG:long_name = ”Longitude of TSG” ;
LONGITUDE_TSG:units = ”degrees_east” ;
LONGITUDE_TSG:valid_min = -180. ;
LONGITUDE_TSG:valid_max = 180. ;
LONGITUDE_TSG:standard_name = ”longitude” ;
LONGITUDE_TSG:_FillValue = -999.f ;
float SSS_TSG(TIME_TSG) ;
SSS_TSG:long_name = ”Drifter SSS” ;
SSS_TSG:units = ”1” ;
SSS_TSG:salinity_scale = ”Practical Salinity Scale(PSS-78)” ;
SSS_TSG:standard_name = ”sea_water_salinity” ;
SSS_TSG:_FillValue = -999.f ;
float SST_TSG(TIME_TSG) ;
SST_TSG:long_name = ”Drifter SST” ;
SST_TSG:units = ”degree Celsius” ;
SST_TSG:standard_name = ”sea_water_temperature” ;

SST_TSG:_FillValue = -999.f ;
float SSS_TSG_FILTERED(TIME_TSG) ;
SSS_TSG_FILTERED:long_name = ”Drifter SSS median filtered at satellite spatial resolution” ;
SSS_TSG_FILTERED:units = ”1” ;
SSS_TSG_FILTERED:salinity_scale = ”Practical Salinity Scale(PSS-78)” ;
SSS_TSG_FILTERED:standard_name = ”sea_water_salinity” ;
SSS_TSG_FILTERED:_FillValue = -999.f ;
float SST_TSG_FILTERED(TIME_TSG) ;
SST_TSG_FILTERED:long_name = ”Drifter SST median filtered at satellite spatial resolution”
;
SST_TSG_FILTERED:units = ”degree Celsius” ;
SST_TSG_FILTERED:standard_name = ”sea_water_temperature” ;
SST_TSG_FILTERED:_FillValue = -999.f ;
float DISTANCE_TO_COAST_TSG(TIME_TSG) ;
DISTANCE_TO_COAST_TSG:long_name = ”Distance to coasts at TSG location” ;
DISTANCE_TO_COAST_TSG:units = ”km” ;
DISTANCE_TO_COAST_TSG:_FillValue = -999.f ;
float PLATFORM_NUMBER_TSG(TIME_TSG) ;
PLATFORM_NUMBER_TSG:long_name = ”TSG unique identifier” ;
PLATFORM_NUMBER_TSG:conventions = ”WMO float identifier : A9IIIII” ;
PLATFORM_NUMBER_TSG:units = ”1” ;
PLATFORM_NUMBER_TSG:_FillValue = -999.f ;
float DATE_Satellite_product(TIME_Sat) ;
DATE_Satellite_product:long_name = ”Central time of satellite SSS file” ;
DATE_Satellite_product:units = ”days since 1990-01-01 00:00:00” ;
DATE_Satellite_product:standard_name = ”time” ;
float LATITUDE_Satellite_product(TIME_TSG) ;
LATITUDE_Satellite_product:long_name = ”Satellite product latitude at TSG location” ;
LATITUDE_Satellite_product:units = ”degrees_north” ;
LATITUDE_Satellite_product:valid_min = -90. ;
LATITUDE_Satellite_product:valid_max = 90. ;
LATITUDE_Satellite_product:standard_name = ”latitude” ;
LATITUDE_Satellite_product:_FillValue = -999.f ;
float LONGITUDE_Satellite_product(TIME_TSG) ;
LONGITUDE_Satellite_product:long_name = ”Satellite product longitude at TSG location” ;
LONGITUDE_Satellite_product:units = ”degrees_east” ;
LONGITUDE_Satellite_product:valid_min = -180. ;
LONGITUDE_Satellite_product:valid_max = 180. ;
LONGITUDE_Satellite_product:standard_name = ”longitude” ;
LONGITUDE_Satellite_product:_FillValue = -999.f ;
float SSS_Satellite_product(TIME_TSG) ;
SSS_Satellite_product:long_name = ”Satellite product SSS at TSG location” ;
SSS_Satellite_product:units = ”1” ;
SSS_Satellite_product:salinity_scale = ”Practical Salinity Scale(PSS-78)” ;
SSS_Satellite_product:standard_name = ”sea_surface_salinity” ;
SSS_Satellite_product:_FillValue = -999.f ;
float SST_Satellite_product(TIME_TSG) ;
SST_Satellite_product:long_name = ”Satellite product SST at TSG location” ;
SST_Satellite_product:units = ”degree Celsius” ;

SST_Satellite_product:standard_name = ”sea_surface_temperature” ;
SST_Satellite_product:_FillValue = -999.f ;
float Spatial_lags(TIME_TSG) ;
Spatial_lags:long_name = ”Spatial lag between TSG location and satellite SSS product pixel center” ;
Spatial_lags:units = ”km” ;
Spatial_lags:_FillValue = -999.f ;
float Time_lags(TIME_TSG) ;
Time_lags:long_name = ”Temporal lag between TSG time and satellite SSS product central time” ;
Time_lags:units = ”days” ;
Time_lags:_FillValue = -999.f ;
float ROSSBY_RADIUS_at_TSG(TIME_TSG) ;
ROSSBY_RADIUS_at_TSG:long_name = ”Baroclinic Rossby radius of deformation (Chelton et al., 1998) at TSG location” ;
ROSSBY_RADIUS_at_TSG:units = ”km” ;
ROSSBY_RADIUS_at_TSG:_FillValue = -999.f ;
float Ascat_daily_wind_at_TSG(TIME_TSG) ;
Ascat_daily_wind_at_TSG:long_name = ”Daily Ascat wind speed module at TSG location” ;
Ascat_daily_wind_at_TSG:units = ”m/s” ;
Ascat_daily_wind_at_TSG:_FillValue = -999.f ;
float CMORPH_3h_Rain_Rate_at_TSG(TIME_TSG) ;
CMORPH_3h_Rain_Rate_at_TSG:long_name = ”3-hourly CMORPH rain rate at TSG location” ;
CMORPH_3h_Rain_Rate_at_TSG:units = ”mm/3h” ;
CMORPH_3h_Rain_Rate_at_TSG:_FillValue = -999.f ;
float Ascat_10_prior_days_wind_at_TSG(TIME_TSG, N_DAYS_WIND) ;
Ascat_10_prior_days_wind_at_TSG:long_name = ”Prior 10 days time series of Ascat wind speed module at TSG location” ;
Ascat_10_prior_days_wind_at_TSG:units = ”m/s” ;
Ascat_10_prior_days_wind_at_TSG:_FillValue = -999.f ;
float CMORPH_10_prior_days_Rain_Rate_at_TSG(TIME_TSG, N_3H_RAIN) ;
CMORPH_10_prior_days_Rain_Rate_at_TSG:long_name = ”Prior 10 days times series of 3-hourly CMORPH Rain Rate at TSG location” ;
CMORPH_10_prior_days_Rain_Rate_at_TSG:units = ”mm/3h” ;
CMORPH_10_prior_days_Rain_Rate_at_TSG:_FillValue = -999.f ;
float SSS_ISAS_at_TSG(TIME_TSG) ;
SSS_ISAS_at_TSG:long_name = ”ISAS SSS (5m depth) at TSG location” ;
SSS_ISAS_at_TSG:units = ”1” ;
SSS_ISAS_at_TSG:salinity_scale = ”Practical Salinity Scale(PSS-78)” ;
SSS_ISAS_at_TSG:standard_name = ”sea_water_salinity” ;
SSS_ISAS_at_TSG:_FillValue = -999.f ;
float SSS_PCTVAR_ISAS_at_TSG(TIME_TSG) ;
SSS_PCTVAR_ISAS_at_TSG:long_name = ”Error on ISAS SSS (5m depth) at TSG location (% variance)” ;
SSS_PCTVAR_ISAS_at_TSG:units = ”%” ;
SSS_PCTVAR_ISAS_at_TSG:_FillValue = -999.f ;
float SSS_WOA13_at_TSG(TIME_TSG) ;
SSS_WOA13_at_TSG:long_name = ”WOA 2013 (DECAV-1deg) SSS (0m depth) at TSG loca-

tion” ;
SSS_WOA13_at_TSG:units = ”1” ;
SSS_WOA13_at_TSG:salinity_scale = ”Practical Salinity Scale(PSS-78)” ;
SSS_WOA13_at_TSG:standard_name = ”sea_surface_salinity” ;
SSS_WOA13_at_TSG:_FillValue = -999.f ;
float SSS_STD_WOA13_at_TSG(TIME_TSG) ;
SSS_STD_WOA13_at_TSG:long_name = ”WOA 2013 (DECAV-1deg) SSS STD (0m depth) at TSG location ” ;
SSS_STD_WOA13_at_TSG:units = ”1” ;
SSS_STD_WOA13_at_TSG:_FillValue = -999.f ;

// global attributes:
:Conventions = ”CF-1.6” ;
:title = ”TSG-GOSUD-Sailing-shipMatch-Up Database” ;
:Satellite_product_name = ”SMOS L3 CATDS CECOS LOCEAN V2.1 9DAYS 25KM” ;
:Satellite_product_spatial_resolution = ”25 km” ;
:Satellite_product_temporal_resolution = ”9 days” ;
:Satellite_product_filename = ”v2.1/9days/SMOS_L3_DEBIAS_LOCEAN_AD_20100116_EASE_09d_25km_v00.nc” ;
:Match-Up_spatial_window_radius_in_km = 25. ;
:Match-Up_temporal_window_radius_in_days = 2. ;
:start_time = ”20100114T000005Z” ;
:stop_time = ”20100118T235026Z” ;
:northernmost_latitude = 77.676f ;
:sourthenmost_latitude = -66.423f ;
:westernmost_longitude = -179.219f ;
:easternmost_longitude = 179.199f ;
:geospatial_lat_units = ”degrees north” ;
:geospatial_lat_resolution = ”25 km” ;
:geospatial_lon_units = ”degrees east” ;
:geospatial_lon_resolution = ”25 km” ;
:institution = ”ESA-IFREMER-ODL” ;
:project_name = ”SMOS Pilote Mission Exploitation Platfrom (Pi-MEP) for salinity” ;
:project_url = ”https://pimep-project.odl.bzh” ;
:license = ”Pi-MEP data use is free and open” ;
:product_version = ”1.0” ;
:keywords = ”Oceans > Ocean Salinity > Sea Surface Salinity” ;
:acknowledgment = ”Please acknowledge the use of these data with the following statement: These data were provided by SMOS Pilote Mission Exploitation Platfrom (Pi-MEP) for salinity” ;
:source = ”v2.1/9days/SMOS_L3_DEBIAS_LOCEAN_AD_20100116_EASE_09d_25km_v00.nc” ;
:references = ”https://pimep-project.odl.bzh” ;
:history = ”Processed on 2018-04-18 using MDB_generator” ;
:date_created = ”2018-04-18 17:09:30” ;
}

2.5 MDB characteristics for the particular in situ/satellite pairs

2.5.1 Number of paired SSS data as a function of time and distance to coast

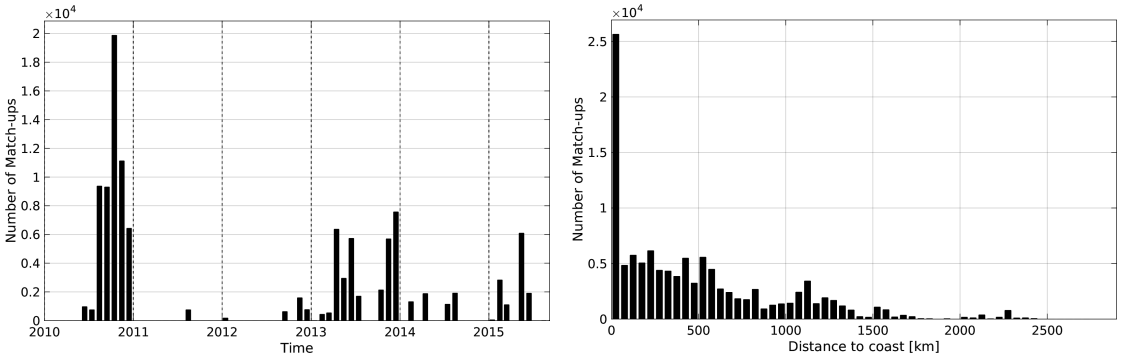

(a) (b)

Figure 1: Number of match-ups between TSG-GOSUD-Sailing-ship and SMOS-L2-DPGS-v662 SSS as a function of time (a) and as function of the distance to coast (b) over the Global Ocean Pi-MEP region and for the full satellite product period.

2.5.2 Histograms of the SSS match-ups

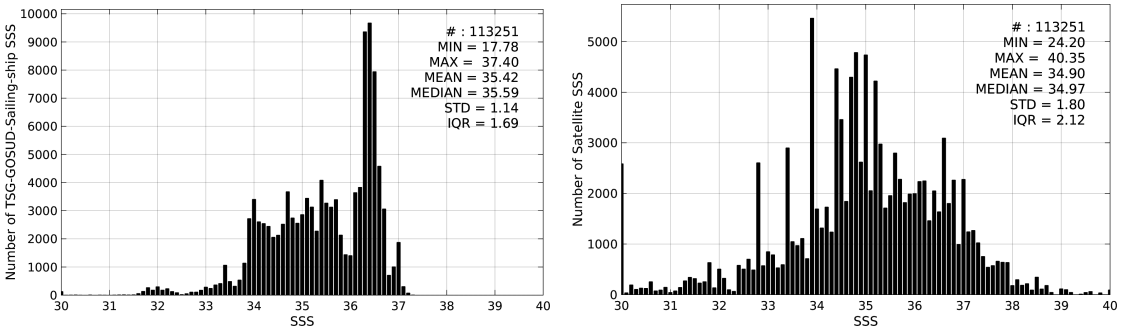

(a) (b)

Figure 2: Histograms of SSS from TSG-GOSUD-Sailing-ship (a) and SMOS-L2-DPGS-v662 (b) considering all match-up pairs per bins of 0.1 over the Global Ocean Pi-MEP region and for the full satellite product period.

2.5.3 Distribution in situ SSS depth in match-ups pairs

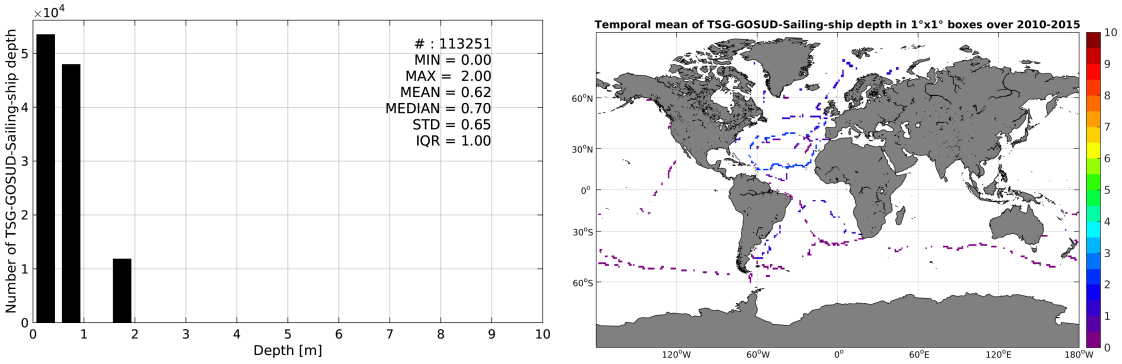

(a) (b)

Figure 3: Histograms of the depth of the upper level SSS measurements from TSG-GOSUD-Sailing-ship in the Match-up DataBase for the Global Ocean Pi-MEP region (a) and temporal mean spatial distribution of pressure of the in situ SSS data over 1°x1° boxes and for the full satellite product period (b).

2.5.4 Spatial Distribution of Match-ups

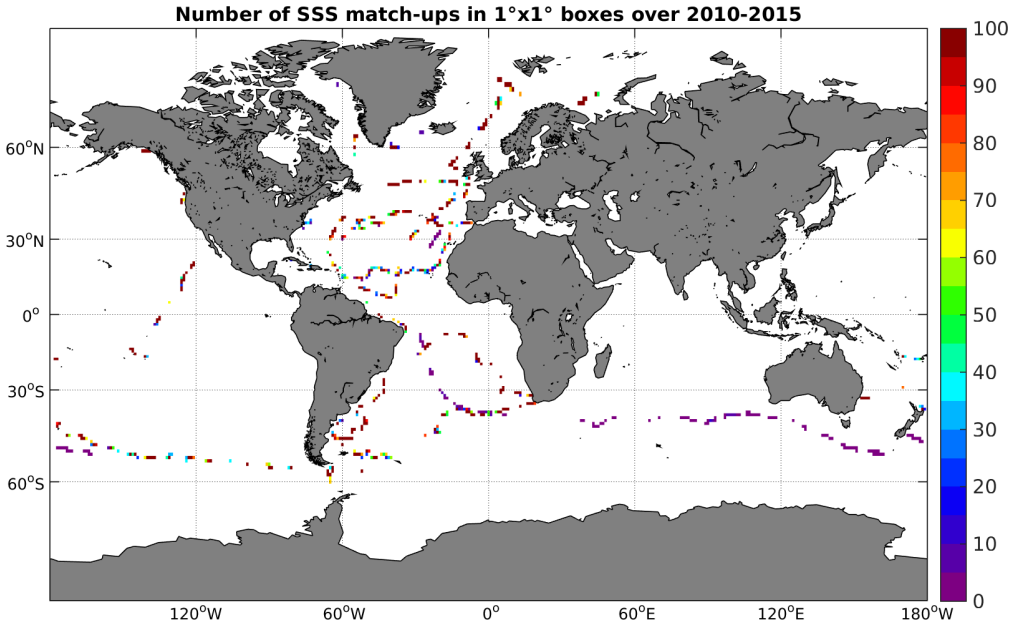

Figure 4: Number of SSS match-ups between TSG-GOSUD-Sailing-ship SSS and the SMOS-L2-DPGS-v662 SSS product for the Global Ocean Pi-MEP region over 1°x1° boxes and for the full satellite product period.

2.5.5 Histograms of the spatial and temporal lags of the match-ups pairs

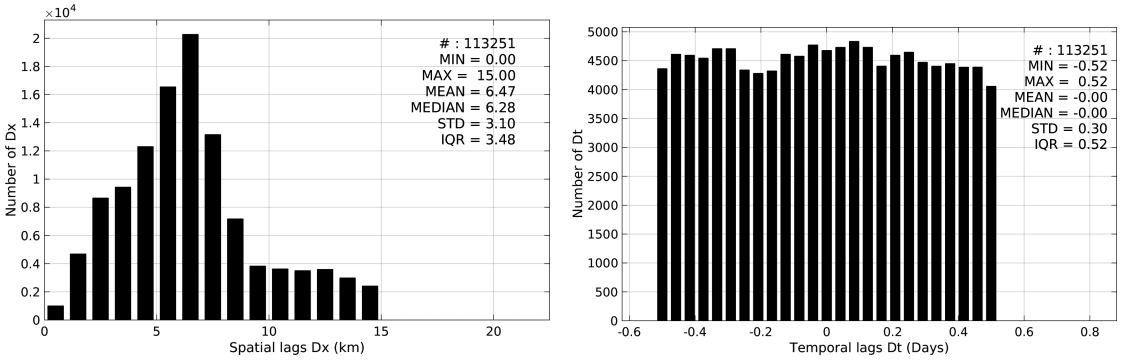

(a) (b)

Figure 5: Histograms of the spatial (a) and temporal (b) lags between the time of the TSG-GOSUD-Sailing-ship measurements and the date of the corresponding SMOS-L2-DPGS-v662 SSS product.

3 MDB file Analyses

3.1 Spatial Maps of the Temporal mean and STD of in situ and satellite SSS and of the difference (ΔSSS)

In Figure 6, we show maps of temporal mean (left) and standard deviation (right) of the SMOS-L2-DPGS-v662 satellite SSS product (top) and of the TSG-GOSUD-Sailing-ship in situ dataset at the collected Pi-MEP match-up pairs. The temporal mean and std are gridded over the full satellite product period and over spatial boxes of size 1°x1°.

At the bottom of Figure 6, the temporal mean (left) and standard deviation (right) of the differences between the satellite SSS product and in situ data found at match-up pairs, namely ΔSSS(Satellite -TSG-GOSUD-Sailing-ship), is also gridded over the full satellite product period and over spatial boxes of size 1°x1°.

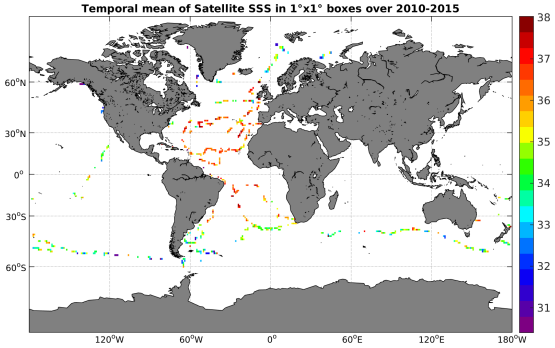

(a) MEAN(Satellite SSS)

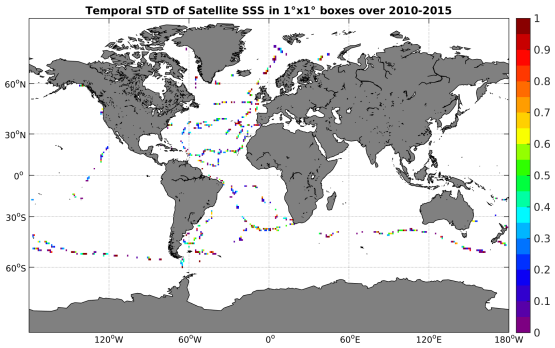

(b) STD(Satellite SSS)

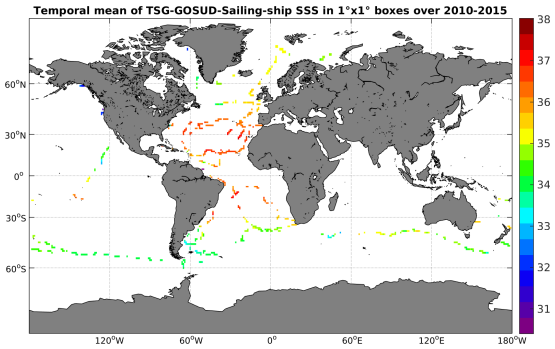

(c) MEAN(TSG-GOSUD-Sailing-ship SSS)

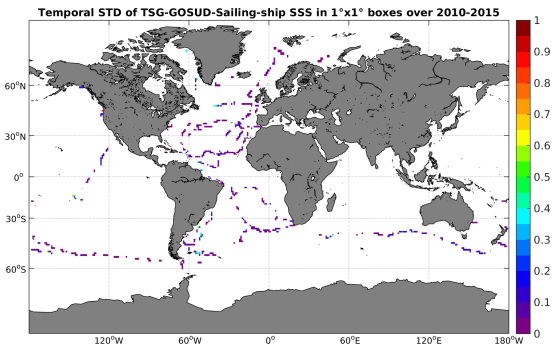

(d) STD(TSG-GOSUD-Sailing-ship SSS)

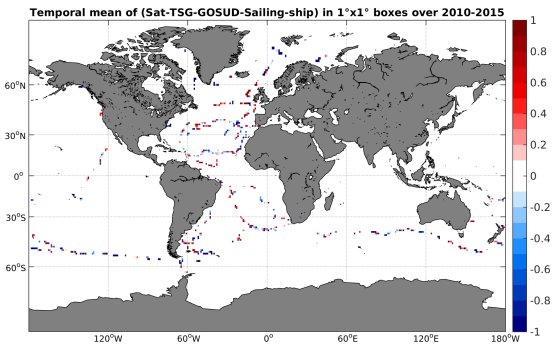

(e) MEAN(ΔSSS) (Satellite - TSG-GOSUD-Sailing-ship)

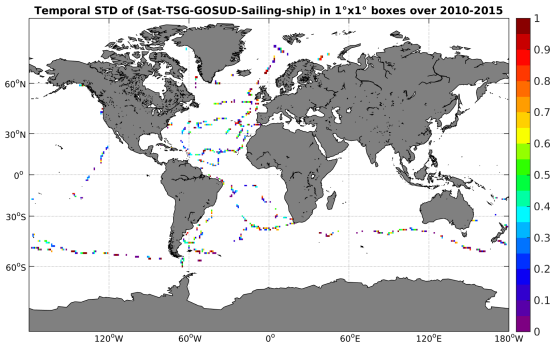

(f) STD(ΔSSS) (Satellite - TSG-GOSUD-Sailing-ship)

Figure 6: Temporal mean (left) and STD (right) of SSS from SMOS-L2-DPGS-v662 (top), TSG-GOSUD-Sailing-ship (middle), and of ΔSSS (Satellite - TSG-GOSUD-Sailing-ship). Only match-up pairs are used to generate these maps.

3.2 Time series of the monthly averaged mean and STD of in situ and satellite SSS and of the (ΔSSS)

In the top panel of Figure 7, we show the time series of the monthly averaged SSS estimated over the full Global Ocean Pi-MEP region for both SMOS-L2-DPGS-v662 satellite SSS product (in black) and the TSG-GOSUD-Sailing-ship in situ dataset (in blue) at the collected Pi-MEP match-up pairs.

In the middle panel of Figure 7, we show the time series of the monthly averaged ΔSSS (Satellite - TSG-GOSUD-Sailing-ship) for the collected Pi-MEP match-up pairs and estimated over the full Global Ocean Pi-MEP region.

In the bottom panel of Figure 7, we show the time series of the monthly averaged standard deviation of the ΔSSS (Satellite - TSG-GOSUD-Sailing-ship) for the collected Pi-MEP match-up pairs and estimated over the full Global Ocean Pi-MEP region.

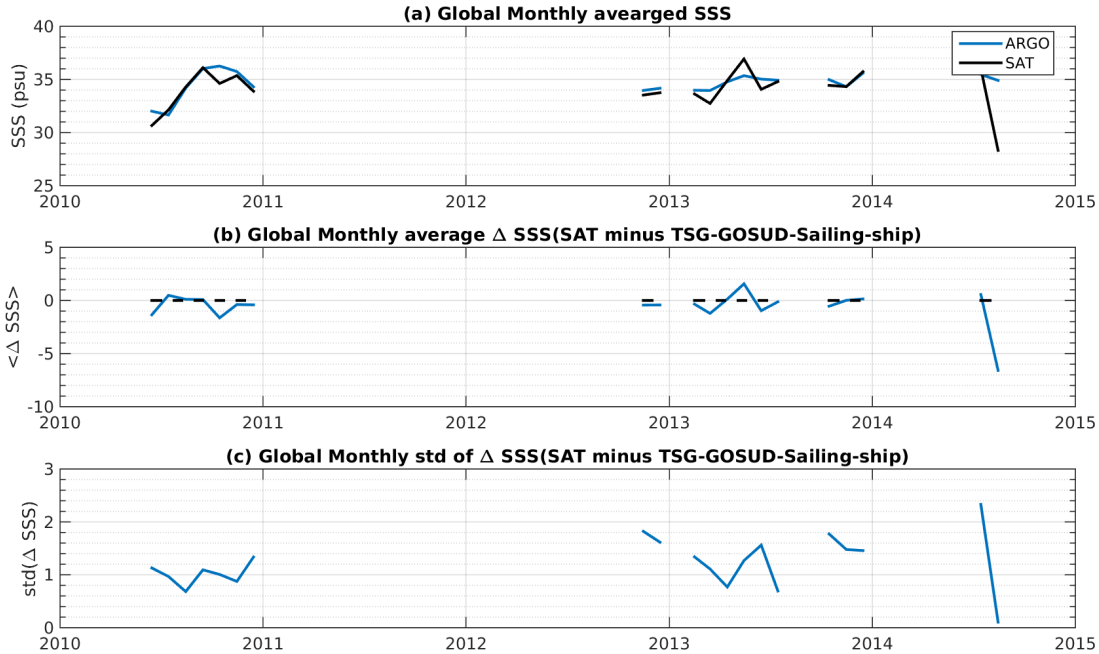

Figure 7: Time series of the monthly averaged mean SSS (top), mean ΔSSS (Satellite - TSG-GOSUD-Sailing-ship) and STD of ΔSSS (Satellite - TSG-GOSUD-Sailing-ship) over the Global Ocean Pi-MEP region considering all match-ups collected by the Pi-MEP platform.

3.3 Zonally-averaged Time-mean and temporal STD of in situ and satellite SSS and of the ΔSSS

In Figure 8 left panel, we show the zonally averaged time-mean SSS estimated at the collected Pi-MEP match-up pairs for both SMOS-L2-DPGS-v662 satellite SSS product (in black) and the TSG-GOSUD-Sailing-ship in situ dataset (in blue). The time mean is evaluated over the full satellite SSS product period.

In the right panel of Figure 8, we show the zonally averaged time-mean ΔSSS (Satellite - TSG-GOSUD-Sailing-ship) for all the collected Pi-MEP match-up pairs estimated over the full satellite product period.

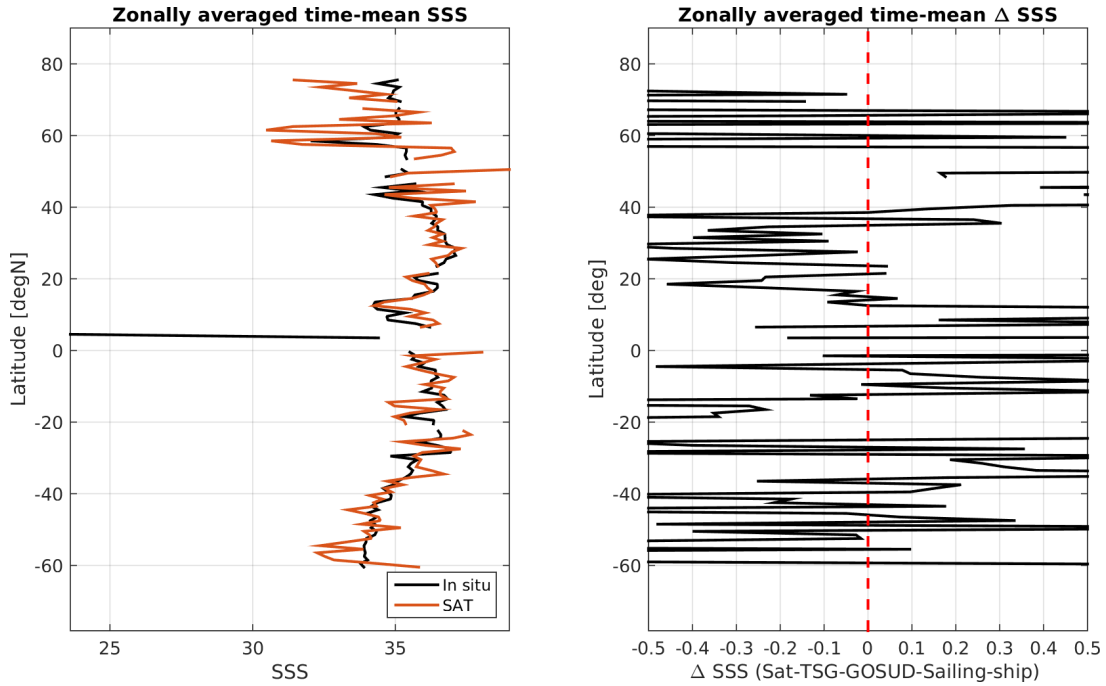

Figure 8: Left panel: Zonally averaged time mean SSS from SMOS-L2-DPGS-v662 (black) and from TSG-GOSUD-Sailing-ship (blue). Right panel: zonally averaged time-mean ΔSSS (Satellite - TSG-GOSUD-Sailing-ship) for all the collected Pi-MEP match-up pairs estimated over the full satellite product period.

3.4 Scatterplots of satellite vs in situ SSS by latitudinal bands

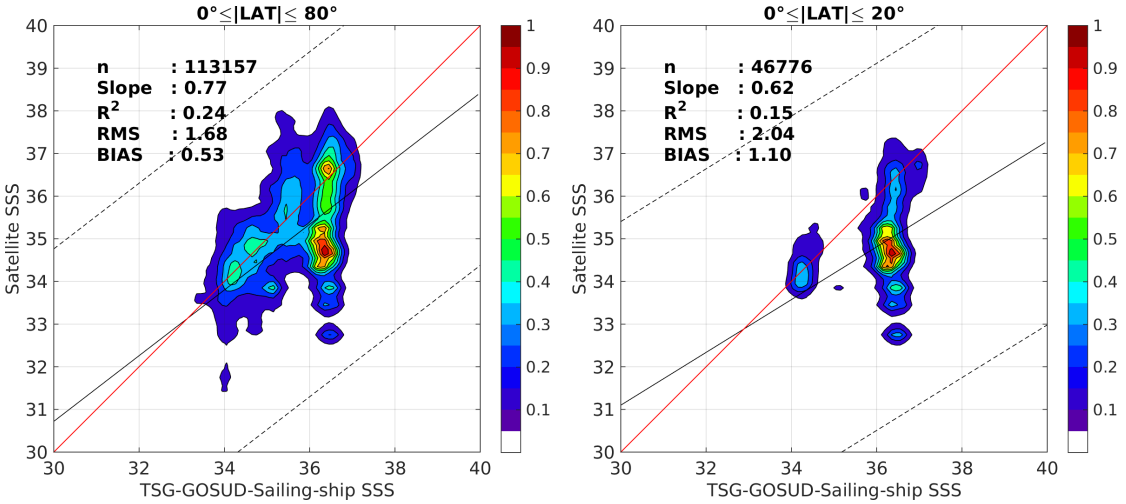

(a) $0° \leq |\text{LAT}| \leq 80°$

(b) $0° \leq |\text{LAT}| \leq 20°$

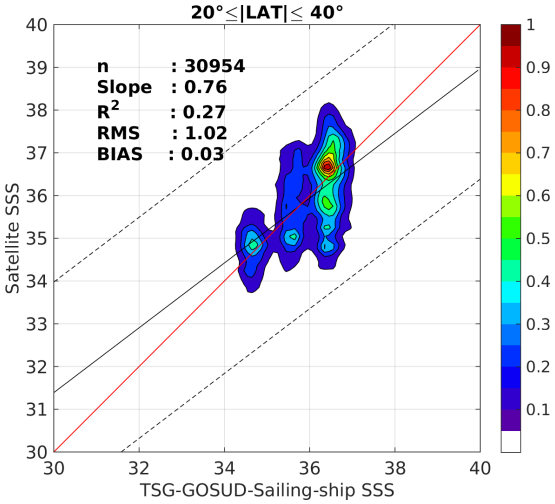

(c) $20° \leq |\text{LAT}| \leq 40°$

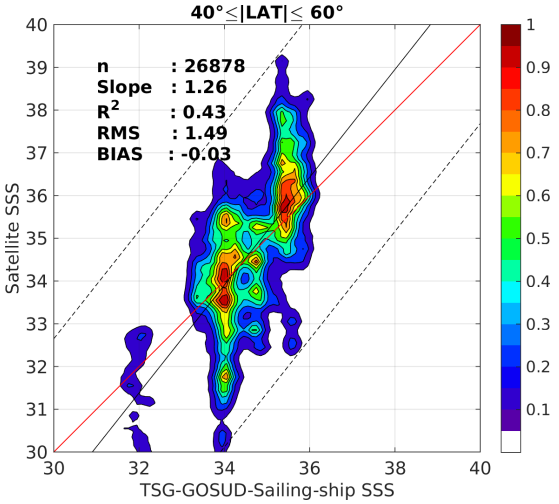

(d) $40° \leq |\text{LAT}| \leq 60°$

Figure 9: Contour maps of the concentration of SMOS-L2-DPGS-v662 SSS (y-axis) versus TSG-GOSUD-Sailing-ship SSS (x-axis) at match-up pairs for different latitude bands. For each plot, the red line shows x=y. The black thin and dashed lines indicate a linear fit through the data cloud and the ±95% confidence levels, respectively. The number match-up pairs n, the slope and R^2 coefficient of the linear fit, the root mean square (RMS) and the mean bias between satellite and in situ data are indicated for each latitude band in each plots.

3.5 Time series of the monthly averaged mean and STD of the ΔSSS sorted by latitudinal bands

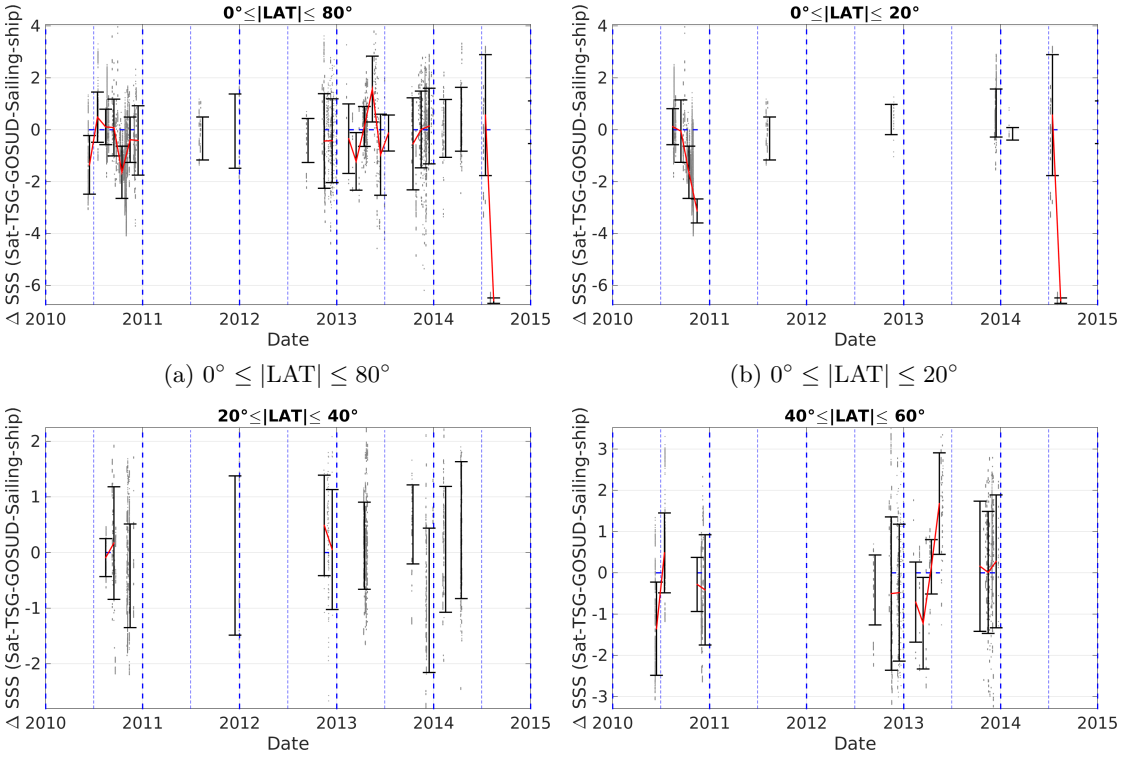

(a) $0° \leq |\text{LAT}| \leq 80°$

(b) $0° \leq |\text{LAT}| \leq 20°$

(c) $20° \leq |\text{LAT}| \leq 40°$

(d) $40° \leq |\text{LAT}| \leq 60°$

Figure 10: Monthly-average mean (red curves) ΔSSS (Satellite - TSG-GOSUD-Sailing-ship) and ±1 STD (black vertical thick bars) as function of time for all the collected Pi-MEP match-up pairs estimated over the Global Ocean Pi-MEP region and for the full satellite product period are shown for different latitude bands: (a) Latitude band 80°S-80°N, (b) latitude band 20°S-20°N, (c) Mid Latitude bands 40°S-20°S and 20°N-40°N and (d) Latitude bands 60°S-40°S and 40°N-60°N.

3.6 ΔSSS sorted as function of geophysical conditions

In Figure 11, we classify the match-up differences ΔSSS (Satellite - in situ) between SMOS-L2-DPGS-v662 and TSG-GOSUD-Sailing-ship SSS as function of the geophysical conditions at match-up points. The mean and std of ΔSSS (Satellite - TSG-GOSUD-Sailing-ship) is thus evaluated as function of the

- in situ SSS values per bins of width 0.2,
- in situ SST values per bins of width 1°C,
- ASCAT daily wind values per bins of width 1 m/s,
- CMORPH 3-hourly rain rates per bins of width 1 mm/h, and,
- distance to coasts per bins of width 50 km.

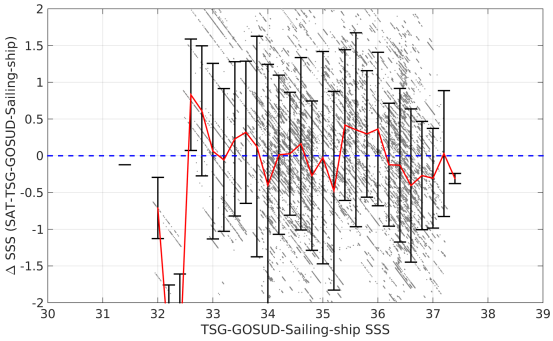

(a) TSG-GOSUD-Sailing-ship SSS

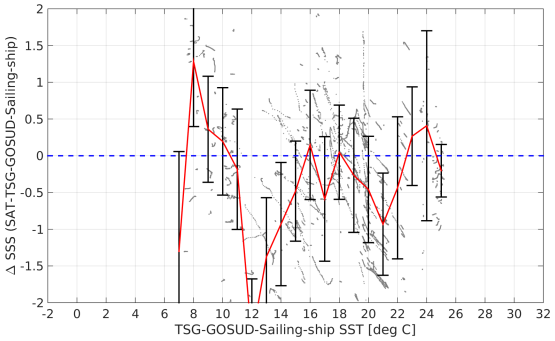

(b) TSG-GOSUD-Sailing-ship SST

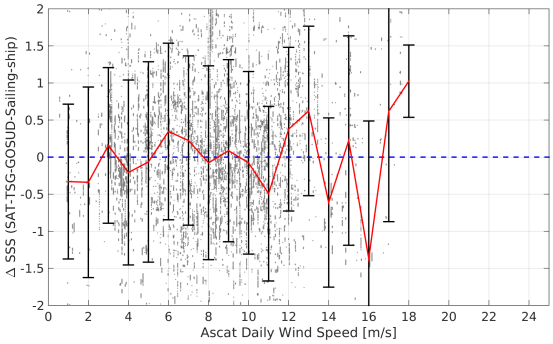

(c) ASCAT Wind Speed

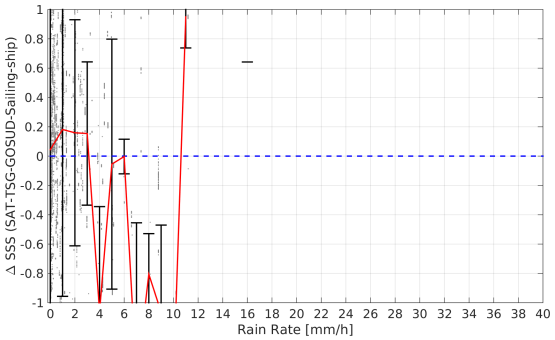

(d) CMORPH Rain rate

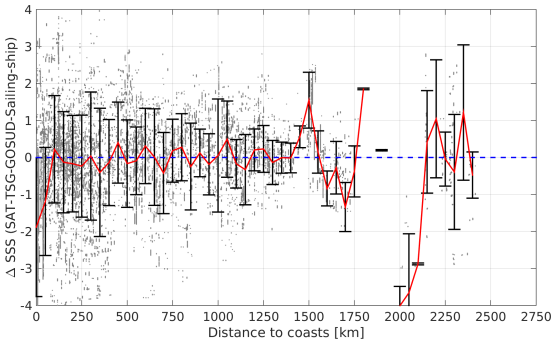

(e) Distance to coast

Figure 11: ΔSSS (Satellite - TSG-GOSUD-Sailing-ship) sorted as function of TSG-GOSUD-Sailing-ship SSS values a), TSG-GOSUD-Sailing-ship SST b), ASCAT Wind speed c), CMORPH rain rate d) and distance to coast (e). In all plots the mean and STD of ΔSSS for each bin is indicated by the red curves and black vertical thick bars (±1 STD)

In Figures 12 and 13, we focus on sub-datasets of the match-up differences ΔSSS (Satellite - in situ) between SMOS-L2-DPGS-v662 and TSG-GOSUD-Sailing-ship for the following specific geophysical conditions:

- **C1**:if the local value at in situ location of estimated rain rate is high (ie. $>$ 10 mm/h) and mean daily wind is low (ie. $<$ 5 m/s).
- **C2**:if the prior 10-days history of the rain and wind at in situ location show high (ie.$>$ 5

mm/h) and low (ie.< 5 m/s) median values, respectively.

- **C3**:if both C1 and C2 are met.
- **C6**:if the in situ data is located where the climatological sss standard deviation is high (ie. above > 0.2).

For each of these conditions, the temporal mean (gridded over spatial boxes of size 1°x1°) and the histogram of the difference ΔSSS (Satellite - in situ) are presented.

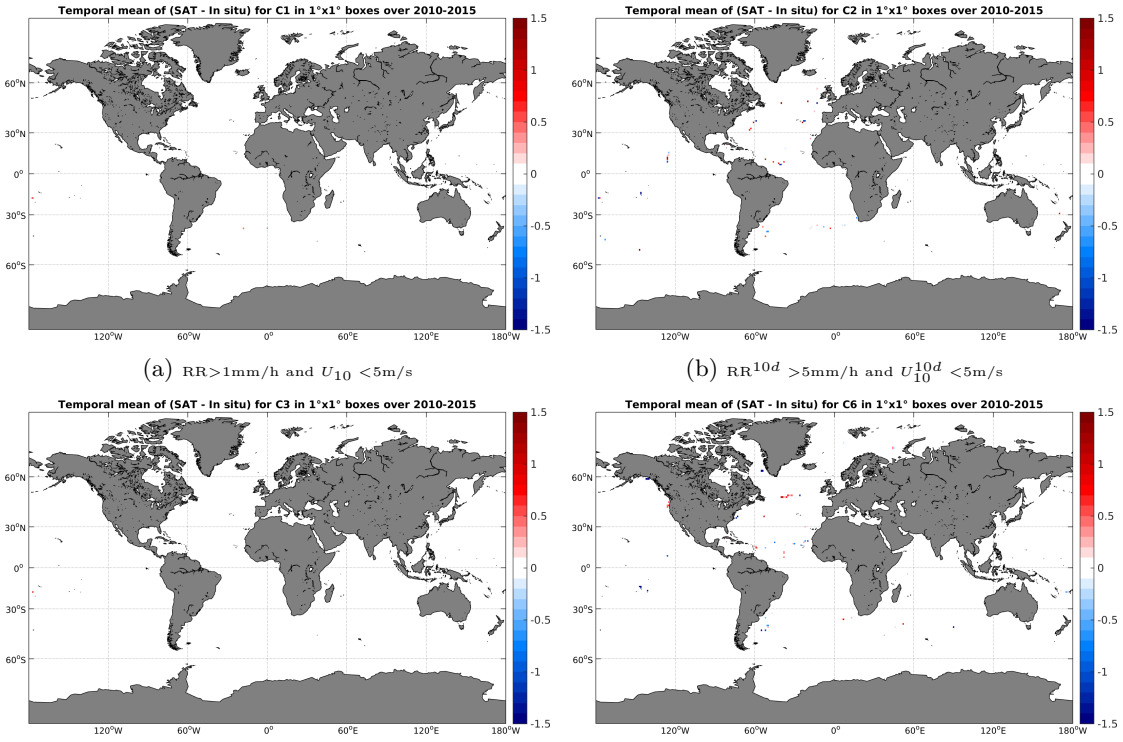

(a) RR>1mm/h and U_{10} <5m/s

(b) RR^{10d} >5mm/h and U_{10}^{10d} <5m/s

(c) C1 U C2

(d) Locations where WOA2013 SSS STD>0.2

Figure 12: Temporal mean gridded over spatial boxes of size 1°x1° of ΔSSS (SMOS-L2-DPGS-v662 - TSG-GOSUD-Sailing-ship) for 4 different subdatasets corresponding to:RR>1mm/h and U_{10} <5m/s (a), RR^{10d} >5mm/h and U_{10}^{10d} <5m/s (b), C1 U C2 (c),Locations where WOA2013 SSS STD>0.2 (d).

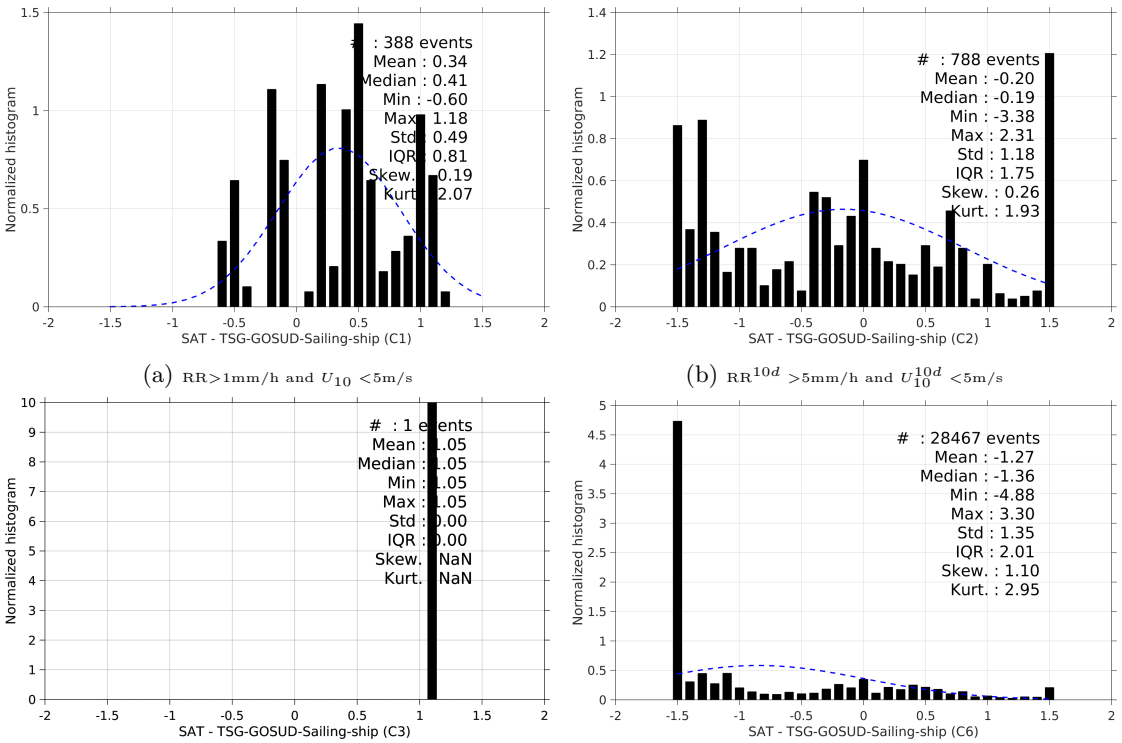

(a) RR>1mm/h and U_{10} <5m/s

(b) RR^{10d} >5mm/h and U_{10}^{10d} <5m/s

(c) C1 U C2

(d) Locations where WOA2013 SSS STD>0.2

Figure 13: Normalized histogram of ΔSSS (SMOS-L2-DPGS-v662 - TSG-GOSUD-Sailing-ship) for 6 different subdatasets corresponding to: RR>1mm/h and U_{10} <5m/s (a), RR^{10d} >5mm/h and U_{10}^{10d} <5m/s (b), C1 U C2 (c), Locations where WOA2013 SSS STD>0.2 (d).

4 Summary

Table 1 presents statistics (mean, median, standard deviation, root mean square and inter-quantile range) of the match-up differences ΔSSS (Satellite - in situ) between SMOS-L2-DPGS-v662 and TSG-GOSUD-Sailing-ship derived over the Global Ocean Pi-MEP region and for the full satellite product period and for the following conditions:

- all: All the match-up pairs satellite/in situ SSS values are used to derive the statistics
- C1: only pairs where RR>1mm/h and U_{10} <5m/s
- C2: only pairs where RR^{10d} >5mm/h and U_{10}^{10d} <5m/s
- C3: only pairs where C1 U C2
- C6: only pairs at Locations where WOA2013 SSS STD>0.2
- C7a: only pairs with a distance to coast < 150 km.
- C7b: only pairs with a distance to coast in the range [150, 800] km.
- C7c: only pairs with a distance to coast > 800 km.

- C8a: only pairs where SST is $< 5°C$.
- C8b: only pairs where SST is in the range [5, 28]°C.
- C8c: only pairs where SST is $> 28°C$.
- C9a: only pairs where SSS is < 33.
- C9b: only pairs where SSS is in the range [33, 37].
- C9c: only pairs where SSS is > 37.

Table 1: Statistics of ΔSSS (Satellite - TSG-GOSUD-Sailing-ship)

Condition	#	Median	Mean	Std	RMS	IQR
all	113251	-0.31	-0.52	1.60	1.68	1.75
C1	388	0.41	0.34	0.49	0.60	0.81
C2	788	-0.19	-0.20	1.18	1.19	1.75
C3	1	1.05	1.05	0.00	1.05	0.00
C6	28467	-1.36	-1.27	1.35	1.85	2.01
C7a	36246	-1.34	-1.35	1.96	2.38	1.81
C7b	51306	-0.09	-0.19	1.29	1.31	1.46
C7c	25699	0.02	-0.01	1.01	1.01	1.05
C8a	0	NaN	NaN	NaN	NaN	NaN
C8b	25757	-0.23	-0.20	1.03	1.05	1.21
C8c	0	NaN	NaN	NaN	NaN	NaN
C9a	2394	0.08	-0.02	1.88	1.88	1.82
C9b	109411	-0.32	-0.54	1.60	1.68	1.77
C9c	1446	-0.35	-0.36	0.54	0.65	0.58

For the same conditions, Table 2 presents statistics of ΔSSS (Satellite - ISAS). Only ISAS SSS values with PCTVAR<80% are used to derive the statistics.

Table 2: Statistics of ΔSSS (Satellite - ISAS)

Condition	#	Median	Mean	Std	RMS	IQR
all	113251	-0.43	-0.58	1.60	1.64	1.83
C1	388	0.27	0.29	0.56	0.63	1.10
C2	788	-0.34	-0.32	1.20	1.24	1.93
C3	1	1.10	1.10	0.00	1.10	0.00
C6	28467	-1.44	-1.42	1.19	1.85	1.30
C7a	33277	-1.44	-1.53	1.71	2.30	1.23
C7b	45232	-0.12	-0.21	1.32	1.34	1.54
C7c	24888	0.06	0.00	0.95	0.95	1.21
C8a	0	NaN	NaN	NaN	NaN	NaN
C8b	22075	-0.20	-0.19	1.08	1.10	1.15
C8c	0	NaN	NaN	NaN	NaN	NaN
C9a	1287	-1.15	-1.11	1.73	2.05	2.36
C9b	100664	-0.42	-0.58	1.54	1.65	1.84
C9c	1446	-0.24	-0.25	0.57	0.63	0.62

References

Abderrahim Bentamy and Denis Croize Fillon. Gridded surface wind fields from Metop/ASCAT measurements. *Int. J. Remote Sens.*, 33(6):1729–1754, March 2012. ISSN 1366-5901. doi: 10.1080/01431161.2011.600348.

Abderrahim Bentamy, Semyon A. Grodsky, James A. Carton, Denis Croizé-Fillon, and Bertrand Chapron. Matching ASCAT and QuikSCAT winds. *J. Geophys. Res.*, 117(C2), February 2012. ISSN 0148-0227. doi: 10.1029/2011JC007479. C02011.

Jaqueline Boutin, Y. Chao, W. E. Asher, T. Delcroix, R. Drucker, K. Drushka, N. Kolodziejczyk, T. Lee, N. Reul, G. Reverdin, J. Schanze, A. Soloviev, L. Yu, J. Anderson, L. Brucker, E. Dinnat, A. S. Garcia, W. L. Jones, C. Maes, T. Meissner, W. Tang, N. Vinogradova, and B. Ward. Satellite and In Situ Salinity: Understanding Near-Surface Stratification and Sub-footprint Variability. *Bull. Am. Meterol. Soc.*, 97(8):1391–1407, 2016. ISSN 1520-0477. doi: 10.1175/bams-d-15-00032.1.

Clément de Boyer Montégut, Gurvan Madec, A. S. Fischer, A. Lazar, and D. Ludicone. Mixed layer depth over the global ocean: An examination of profile data and a profile-based climatology. *J. Geophys. Res.*, 109(C12):C12003, December 2004. ISSN 0148-0227. doi: 10.1029/2004jc002378.

Clément de Boyer Montégut, Juliette Mignot, Alban Lazar, and Sophie Cravatte. Control of salinity on the mixed layer depth in the world ocean: 1. General description. *J. Geophys. Res.*, 112(C6):C06011, June 2007. ISSN 0148-0227. doi: 10.1029/2006jc003953.

Ralph R. Ferraro. Ssm/i derived global rainfall estimates for climatological applications. *J. Geophys. Res.*, 1021:16715–16736, 07 1997. doi: 10.1029/97JD01210.

Ralph R. Ferraro, Fuzhong Weng, Norman C. Grody, and Limin Zhao. Precipitation characteristics over land from the NOAA-15 AMSU sensor. *Geophys. Res. Lett.*, 27(17):2669–2672, 2000. doi: 10.1029/2000GL011665.

Fabienne Gaillard, E. Autret, V. Thierry, P. Galaup, C. Coatanoan, and T. Loubrieu. Quality Control of Large Argo Datasets. *J. Atmos. Oceanic Technol.*, 26(2):337–351, 2012/10/10 2009. doi: 10.1175/2008JTECHO552.1.

Fabienne Gaillard, Thierry Reynaud, Virginie Thierry, Nicolas Kolodziejczyk, and Karina von Schuckmann. In Situ-Based Reanalysis of the Global Ocean Temperature and Salinity with ISAS: Variability of the Heat Content and Steric Height. *J. Clim.*, 29(4):1305–1323, February 2016. ISSN 1520-0442. doi: 10.1175/jcli-d-15-0028.1.

Robert J. Joyce, John E. Janowiak, Phillip A. Arkin, and Pingping Xie. CMORPH: A Method that Produces Global Precipitation Estimates from Passive Microwave and Infrared Data at High Spatial and Temporal Resolution. *J. Hydrometeorol.*, 5(3):487–503, June 2004. ISSN 1525-7541. doi: 10.1175/1525-7541(2004)005⟨0487:camtpg⟩2.0.co;2.

Nicolas Kolodziejczyk, Gilles Reverdin, and Alban Lazar. Interannual Variability of the Mixed Layer Winter Convection and Spice Injection in the Eastern Subtropical North Atlantic. *J. Phys. Oceanogr.*, 45(2):504–525, Feb 2015. ISSN 1520-0485. doi: 10.1175/jpo-d-14-0042.1.

Christian Kummerow, Y. Hong, W. S. Olson, S. Yang, R. F. Adler, J. McCollum, R. Ferraro, G. Petty, D-B. Shin, and T. T. Wilheit. The Evolution of the Goddard Profiling Algorithm

(GPROF) for Rainfall Estimation from Passive Microwave Sensors. *J. Appl. Meteorol.*, 40(11): 1801–1820, 2001. doi: 10.1175/1520-0450(2001)040⟨1801:TEOTGP⟩2.0.CO;2.

Thierry Reynaud, Floriane Desprez De Gesincourt, Fabienne Gaillard, Hervé Le Goff, and Gilles Reverdin. Sea Surface Salinity from Sailing ships : Delayed mode dataset, annual release, 2015. doi: 10.17882/39476.